PAPER

A comparative analysis of the bistability switch for platelet aggregation by logic ODE based dynamical modeling†

Marcel Mischnik,*[a] Stepan Gambaryan,[bc] Hariharan Subramanian,[b] Jörg Geiger,[b] Claudia Schütz,[b] Jens Timmer[de] and Thomas Dandekar*[a]

A kinetic description of the fragile equilibrium in thrombozytes regulating blood flow would be an important basis for rational medical interventions. Challenges for such a model include regulation by a complex bistability switch that determines the transition from reversible to irreversible aggregation and sparse data on the kinetics. A so far scarcely applied technique is given by the derivation of ordinary differential equations from Boolean expressions, which are called logic ODEs. We employ a combination of light-scattering based thrombocyte aggregation data, western blot and calcium measurements to compare three different ODE approaches regarding their suitability to achieve a data-consistent model of the switch. Our analysis reveals the standardized qualitative dynamical system approach (SQUAD) to be a better choice than classical mass action formalisms. Furthermore, we analyze the dynamical properties of the platelet aggregation threshold as a basis for medical interventions such as novel platelet aggregation inhibitors.

Introduction

Platelet aggregation

Platelets play a key role in normal and pathological hemostasis through their ability to rapidly adhere to activated or injured endothelium, subendothelial matrix proteins and other activated platelets thus forming stable aggregates.[1] They combine major roles in the development and progression of cardiovascular diseases, and have emerged as one of the most important cellular therapeutic targets since they are now considered key mediators of thrombosis, inflammation, and atherosclerosis. This is supported by a wealth of evidence from large clinical trials, where established anti-platelet drugs have become paramount in the prevention and management of various diseases involving the cardiovascular, cerebrovascular, and peripheral arterial systems.[2] This has triggered interest and efforts to improve both the diagnostic and therapeutic aspects of platelet function in disease.[3,4]

One of the most important physiological platelet activators is adenosine diphosphate (ADP), which is secreted by activated platelets representing a very important amplification mechanism to recruit additional platelets to sites of vascular injury. ADP has two G-protein-coupled receptors (P2Y1 and P2Y12) in the platelet plasma membrane. Activation of the 7-transmembrane domain receptor P2Y1 stimulates calcium mobilization, platelet shape change, and rapid and reversible platelet aggregation. Stimulation of the P2Y12 receptor coupled to both Gs and Gi proteins enhances amplification of stable platelet aggregation and secretion. The transition between reversible and irreversible aggregation is thereby characterized by a bistable threshold behaviour, that integrates the signals from all receptors and generates an output, that manifests in the activation rate of the fibrinogen receptor integrin α2bβ3. Understanding the dynamical properties of this threshold behaviour is a pivotal aspect for the development of novel diagnostics and anti-thrombotic therapies.

Mathematical modeling and parameter estimation in logic ODEs

Mathematical modeling is a powerful tool to examine quantitative features of complex systems, and we apply it here to the platelet aggregation bistability switch. Classical ODE-based approaches

[a] *Department of Bioinformatics, Biocenter, Am Hubland, 97074 Wuerzburg, Germany. E-mail: marcel.mischnik@gmail.com, dandekar@biozentrum.uni-wuerzburg.de; Fax: +49 931 888 4552; Tel: +49 931 318 4551*

[b] *Institute for Clinical Biochemistry & Pathobiochemistry, Grombuehlstraße 12, 97080 Wuerzburg, Germany. E-mail: s.gambaryan@klin-biochem.uni-wuerzburg.de, joerg.geiger@uni-wuerzburg.de; Fax: +49 931 201 647 000; Tel: +49 931 201 47 010*

[c] *Sechenov Institute of Evolutionary Physiology and Biochemistry, Russian Academy of Sciences, 194223 St. Petersburg, Russia*

[d] *Institute of Physics, Hermann-Herder-Strasse 3a, 79104 Freiburg, Germany. E-mail: jeti@fdm.uni-freiburg.de; Fax: +49 761 203 8541; Tel: +49 761 203 8532*

[e] *BIOSS Centre for Biological Signalling Studies, Schaenzlestrasse 18, 79104 Freiburg, Germany*

† Electronic supplementary information (ESI) available. See DOI: 10.1039/c4mb00170b

use mass action or Michaelis–Menten kinetics to model biochemical reactions. Regarding platelets, one challenge is that detailed kinetic data on all components of the system are difficult to come about. Hence, only Boolean discrete models achieved a broader description of central platelet activatory and inhibitory pathways so far.[5] All more ambitious efforts lack sufficient kinetic data and hence, other previous modeling papers looked at other aspects of thrombosis and hemostasis.[6–9] However, there is an alternative available to model the complex switch in platelet aggregation, given by logical ODEs: some effort has been made to derive differential equations from Boolean expressions (AND, OR, NOT), using the standardized qualitative dynamical systems approach[10] or HillCube equations.[11] The resulting formulae are called logic ODEs. They display transitions between the discrete truth values 0 and 1 as continuous functions and abstain from including detailed information about underlying reaction kinetics. However, the application of parameter estimation methods to calibrate the quantitative effects of activators or inhibitors on a given node within these approaches is up to now scarce, it was not clear which formalism would work best with our data.

For the analysis of platelet aggregation we therefore conducted a comparison between models built by (a) the standardized qualitative dynamical systems approach, (b) HillCube equations and (c) mass action kinetics. All three models were subjected to multi-experiment fitting along a combination of low angle light scattering analysis (LASCA), western-blot and calcium measurement data. The differential equations of all three models can be found in the ESI.†

Model topology

The input layer of the models is built by the ADP receptors P2Y1 and P2Y12, and the thromboxan receptor (ThromR). ADP binding to the P2Y1 receptor leads to an opening of intracellular calcium channels and thereby to an increase of the cytosolic calcium concentration, which results in the activation of the small GTPase Rap1. Rap1 is a direct activator of the fibrinogen receptor integrin α2bβ3 (Int), whose activation is proportional to the aggregation rate, thus representing the model's output node. Nevertheless, the activation of integrin has two important effects in our model: It triggers the mobilization of Src-kinase associated to its cytoplasmatic domain, and induces the synthesis and release of autocrin thromboxan, which is then secreted and bound by its own receptor ThromR. ThromR signals back to integrin, establishing a positive feedback loop.

Ligand binding to P2Y12 on the other hand leads to engagement of PI3-kinase, which in turn activates Akt-kinase via phosphorylation. Akt embodies a third activator of integrin.

To capture the observed threshold properties of platelet aggregation, we included a bistability switch consisting of Src-kinase and a set of tyrosine phosphatases. Src is thereby mobilized by integrin and capable of self-activation via autophosphorylation at tyr-418, as well as inactivation of the tyrosine phosphatases. Those in return activate themselves and inactivate Src through dephosphorylation. The state of the bistability switch represents an input for Akt-kinase, which forwards the signal to integrin, building a second positive feedback-loop.
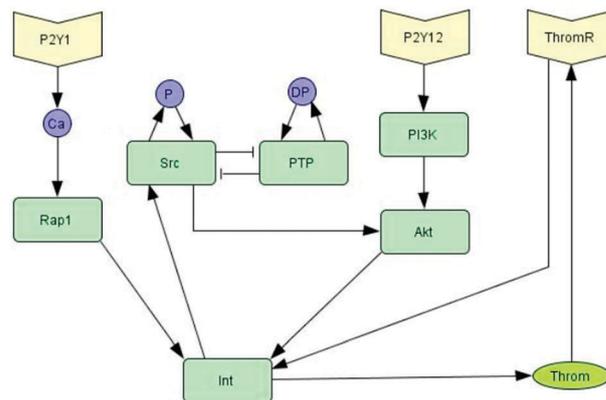

Fig. 1 Network topology. The receptor layer consists of the two ADP receptors P2Y1 and P2Y12 and the thromboxane receptor ThromR. Ligand binding to P2Y1 leads via opening of intracellular calcium channels to the activation of Rap1 and thus to an inside-out signaling that results in a conformational change of integrin α2bβ3 leading to aggregation. Engagement of P2Y12 causes phosphorylation events that result in the activation of Akt kinase, which also transmits the signal to integrin. A positive feedback loop including a bistability switch built of Src kinase and a set of tyrosine phosphatases that is activated upon integrin outside-in signaling determines the transition from reversible to irreversible aggregation (black arrows: activation, blunt ends: inhibition, P: autophosphorylation, DP: autodephosphorylation, Ca: calcium, Int: integrin α2bβ3, Src: sarcoma tyrosine kinase, PTP: tyrosine phosphatases, PI3K: phosphoinositide-3 kinase, Akt: protein kinase B, Throm: thromboxane A2, ThromR: thromboxane A2 receptor).

The dynamics established by the described Src-PTP interplay constitute the focus of this modeling approach. Fig. 1 illustrates the network topology valid for all three implemented models. Additional information about the mathematical formalisms can be found in the methods section.

Methods

In silico modeling

The models consist of a set of ordinary differential equations, representing concentration changes over time. We analysed three different implementations of the respective equations, being mass action, HillCube, and the standardized qualitative dynamical systems approach. All basal concentrations and parameter values can be found in the ESI.†

Mass action. In the mass action approach, all concentration changes over time are implemented as

$$\frac{\mathrm{d}x}{\mathrm{d}t} = \prod_{i=1}^{n} r_i \cdot \sum_{j=1}^{m} \left(a_j \cdot k_j \right)$$

with r_i being the i-th reactant from which a node is built, a_j the j-th modifier catalyzing the reaction, and k_j the j-th rate constant belonging to each modifier. Fitted parameters include the activation and deactivation constants of all incorporated proteins, the calcium release and re-uptake rates, as well as the basal concentrations of all active and inactive players, and scaling factors for the observables integrin, Akt, calcium and Rap1. To account for the quantitatively different ligand effects

in platelet rich plasma (PRP) and washed platelets, we estimated the ADP input concentration for the calcium, Akt and Rap1 detections together with the other parameters.

SQUAD. In the standardized qualitative dynamical systems approach the differential equations represent logistic functions that guarantee a monotonic behaviour within the closed interval [0,1] and have a shape according to

$$\frac{\mathrm{d}x_i}{\mathrm{d}t} = \frac{-\mathrm{e}^{0.5h} + \mathrm{e}^{-h(\omega_i - 0.5)}}{(1 - \mathrm{e}^{0.5h})(1 + \mathrm{e}^{-h(\omega_i - 0.5)})} - \gamma_i x_i$$

$$\omega_i = \begin{cases} \left(\dfrac{1 + \sum \alpha_n}{\sum \alpha_n}\right)\left(\dfrac{\sum \alpha_n x_n^{\mathrm{a}}}{1 + \sum \alpha_n x_n^{\mathrm{a}}}\right) & \\ \quad \times \left(1 - \left(\dfrac{1 + \sum \beta_m}{\sum \beta_m}\right)\left(\dfrac{\sum \beta_m x_m^i}{1 + \sum \beta_m x_m^i}\right)\right) & \S \\ \left(\dfrac{1 + \sum \alpha_n}{\sum \alpha_n}\right)\left(\dfrac{\sum \alpha_n x_n^{\mathrm{a}}}{1 + \sum \alpha_n x_n^{\mathrm{a}}}\right) & \S\S \\ \left(1 - \left(\dfrac{1 + \sum \beta_m}{\sum \beta_m}\right)\left(\dfrac{\sum \beta_m x_m^i}{1 + \sum \beta_m x_m^i}\right)\right) & \S\S\S \end{cases}$$

$0 \leq x_i \leq 1$

$0 \leq \omega_i \leq 1$

$h, \alpha_n, \beta_m, \gamma_i > 0$

$\{x_n^{\mathrm{a}}\}$ is the set of activators of x_i

$\{x_n^i\}$ is the set of inhibitors of x_i

$\S$ is used if x_i has activators and inhibitors

$\S\S$ is used if x_i has only activators

$\S\S\S$ is used if x_i has only inhibitors

with a_n being the effect of the n-th activator and b_m the m-th inhibitor of node x^i. Fitted parameters include all modifier effects, the average Hill-coefficient of the system $\bar{h}$, the basal concentrations of Src and PTP, as well as scaling factors for Akt, calcium and Rap1 and inputs for ADP.

HillCube. In the HillCube approach, we assume the production of X_i to be given by $\bar{B}_i$, and the degradation to be proportional to $\bar{x}_i$. Then the development of $\bar{x}_i$ over time is governed by the ordinary differential equation (ODE)

$$\dot{X}_i = \frac{1}{\tau_i}(\bar{B}_i(\bar{X}_{i1}, \bar{X}_{i2}, \ldots, \bar{X}_{iN_i}) - \bar{X}_i),$$

where τ_i can be interpreted as the life-time of species X_i. Then we define the functions

$$\bar{B}_i^{\mathrm{I}}(\bar{X}_{i1}, \bar{X}_{i2}, \ldots, \bar{X}_{iN_i})$$

by linear interpolation of Boolean functions using the technique of multivariate polynomial interpolation as explained in Wittmann *et al.* (2009).[11] These functions are called BooleCubes. The functions $\bar{B}_i^{\mathrm{I}}$ are affine multilinear, *i.e.* for each $1 \leq j \leq N_i$ and fixed $\bar{x}_{ik}, k \neq j$, there exist constants $a, b \in \mathbb{R}$ such that

$$\bar{B}_i^{\mathrm{I}}(\bar{X}_{i1}, \bar{X}_{i2}, \ldots, \bar{X}_{iN_i}) = a + b\bar{X}_{ij}$$

Molecular interactions, however, are known to show a switch-like behavior, which can be modeled using sigmoid shaped Hill functions.

$$f(\bar{X}) = \bar{X}^n / (\bar{X}^n + k^n)$$

The Hill coefficient n determines the slope of the curve and is a measure of the cooperativity of the interaction. The parameter k corresponds to the threshold in the Boolean model, above which one defines the state of a species as 'on'. Mathematically speaking, it is the value at which the activation is half maximal. We now define a Hill function f_{ij} with parameters n_{ij} and k_{ij} for every interaction and define new functions

$$\bar{B}_i^{\mathrm{H}}(\bar{X}_{i1}, \bar{X}_{i2}, \ldots, \bar{X}_{iN_i}) := \bar{B}_i^{\mathrm{I}}(f_{i1}(\bar{X}_{i1}), f_{i2}(\bar{X}_{i2}), \ldots, f_{iN_i}(\bar{X}_{iN_i})),$$

which are called HillCubes.[11] Fitted parameters for this approach include all τ_i and k_{ij} as well as basal concentrations, scaling parameters and inputs as stated for the SQUAD model. The average Hill-coefficient was fixed to 1 for numerical reasons.

Parameter estimation

Determining model parameters that optimize the χ^2-merit function and set the model statistically compliant with the available data is a fundamental problem. To fit the model

$$y = y(t_i, \vec{p})$$

to data, we optimize the χ^2-merit function

$$\chi^2(\vec{p}) = \sum \frac{y_i - y(t_i, \vec{p})}{\sigma^2}$$

with y_i representing data point i with standard deviation σ_i. The model value at time point i for a set of parameter values $\vec{p}$ is given by $y(t_i, \vec{p})$. Assuming normally distributed measurement errors, this corresponds to a maximum likelihood estimation. To optimize this function, we used the trust region algorithm in logarithmic parameter space,[12] a powerful deterministic least-square optimizer. ODE-integration was thereby performed by means of SVODES.[13]

The models were optimized by fitting them 1000 times simultaneously to LASCA-based aggregation, western-blot and calcium measurements after various stimuli, each time varying all parameters by latin hypercube sampling. The magnitude of the measurement error for each observable was estimated along with the remaining parameters. Therefore, a parameterized error model of the form

$$\sigma(t, \theta) = s(y(t, \theta), \theta)$$

describing the measurement noise for each model output was assumed. The additional parameters accounting for the magnitude of the measurement noise were estimated simultaneously with the remaining model parameters.

Corresponding differential equations were implemented and further analyzed using the MATLAB toolbox PottersWheel.[14]

Profile likelihood

The idea of profile likelihood is to explore the parameter space for each parameter in the direction of the least increase in χ^2. It is calculated for each parameter individually by

$$\chi_{\mathrm{PL}}^2(p_i) = \min_{p_{j \neq i}} \left[\chi^2(p) \right]$$

meaning re-optimization of $\chi^2(p)$ with respect to all parameters $p_{j \neq i}$, for each value of parameter p_i. Hence, the profile likelihood keeps χ^2 as small as possible alongside p_i. Structural non-identifiable parameters are characterized by a flat profile likelihood. The profile likelihood of a practically non-identifiable parameter has a minimum, but is not excessing a threshold α for increasing and/or decreasing values of p_i. In contrast, the profile likelihood of an identifiable parameter exceeds α for both increasing and decreasing values of p_i. The points of passover represent likelihood-based confidence intervals.[15]

Experimental procedures

Platelets were used as washed platelets (WP) resuspended in phosphate buffered saline (PBS, 137 mM NaCl, 2.7 mM KCl, 10 mM Na_2HPO_4, 2 mM KH_2PO_4, pH = 7.4), depending on the assay applied, and prepared from whole human blood.

Whole human blood was obtained from healthy volunteers who had not taken any medication affecting platelet function within 2 weeks prior to the experiment after informed consent according to the declaration of Helsinki and our institutional guidelines and as approved by the local ethics committee. Our studies with human platelets were approved and reconfirmed (September 24, 2008) by the local ethics committee of the University of Würzburg (studies 67/92 and 114/04). The blood was drawn by venipuncture and collected in 1/5 volume of HEPES–citrate buffer (120 mM NaCl, 20 mM sodium citrate, 4 mM KCl, 1.5 mM citric acid, 30 mM D-glucose, 8 mM HEPES, pH = 6.5) and centrifuged at $300 \times g$ for 20 minutes at 20 °C to obtain platelet rich plasma (PRP). For the preparation of washed platelets the PRP was diluted 1 : 1 with HEPES–citrate buffer, apyrase (1 U ml^{-1}) added and centrifuged again at 100 g for 10 min at 20 °C. The pellet was discarded and the supernatant was centrifuged at 380 g for 10 minutes. The resulting pellet was resuspended in HEPES/citrate, left resting for 5 minutes and centrifuged again at 380 g for 10 minutes. The platelet pellet was resuspended in PBS buffer to a cell density of 3×10^5 platelets per ml and apyrase (0.1 U ml^{-1}) added. Washed platelets were used in 200 ml portions. The samples were incubated with the reagents in the water bath at 37 °C as indicated, stopped and treated appropriately for the respective analyte. The reagents were solved in PBS unless otherwise stated.

The experiments described in this manuscript can only be carried out *ex vivo*. The experimental conditions used are as close to the physiological situation as possible, however disregarding interaction with blood cells, vascular cells and vascular factors, fluid mechanics and other physiological variables. In fact any processing of primary cells affects the properties and behavior of these cells fundamentally. Consequently an authentic physiological setting is unachievable. Together with other well-respected researchers in the field (J. Heemskerk, S. Watson, U. Walter) of thrombosis research we have agreed on standard protocols, based on the procedures above. The methods enable reproducible and comparable analysis of platelet function and furnish meaningful data as closely related to the physiological situation as possible (see ref. 9 for further details).

Intracellular calcium regulation was determined fluorometrically with the fluorescent indicator Fura-2. Briefly, platelet rich plasma was incubated with 4 mM Fura-2/AM (di-methyl sulfoxide (DMSO) 1% v/v) for 45 minutes, centrifuged at 350 g and the resulting platelet pellet resuspended in HEPES buffer (150 mM NaCl, 5 mM KCl, 1 mM $MgCl_2$, 10 mM D-glucose, 10 mM HEPES, pH 7.4). The calcium transients were observed in a Perkin-Elmer LS50 luminescence spectrophotometer at an excitation wavelength of 340 nm and an emission wavelength of 510 nm. Data were recorded as relative changes in the Fura-2 fluorescence signal. An absolute quantification of intracellular ion concentrations by fluorometric measurement is, though frequently claimed, virtually impossible. The numerous variables impacting fluorescence quantum efficiency and disturbances in the setting seriously distort the measurement. For this reason we refrain here from calculating dubious absolute calcium concentrations and rather provide data on the relative change of free intracellular calcium concentration.

Western-blot and GTP-pulldown assays were performed as stated in Subramanian *et al.* (2013).[16]

Light scattering experiments were carried out as described in Mindukshev *et al.* (2012).[17]

The data were collected from 3–7 individuals and replicated at least 3 times each. For each individual the mean of the replicates for each time point was calculated. The means of all experiments were pooled.

Results and discussion

Logic *vs.* classic ODEs

We applied three different approaches to model the available experimental data and compared the respective χ^2-values after parameter estimation. In the first and second approach logic ODEs were employed by utilizing the standardized qualitative dynamical systems approach (model 1) and HillCube equations (model 2). Model 3 was implemented by commonly used mass action kinetics for all reactions. For the first two cases we applied self-written Matlab scripts that convert a given network topology into a set of differential equations of the respective form and produce model definition files that can directly be loaded into the Matlab toolbox PottersWheel[14] for parameter estimation and further analyses. Both scripts can be found in the ESI† and are available for download. For large networks the concatenated form of the equations derived from the logical connectivity of the different network layers may become complex and numerically demanding and their biochemical parameters may become difficult to interpret. However, none of these potential limitations applied in our case of platelet

threshold behaviour. The unknown model parameters were estimated by a combination of aggregation measurements by light scattering, calcium detection and quantitative western-blot data. In order to account for the difference between platelet rich plasma (PRP) and washed platelets as well as the slightly distinct effects of a certain input concentration in different methods, we included for each experimental procedure a scaling factor for the applied ADP concentration which was scaled to be between 0.1 and 1. The inputs were implemented as step-functions jumping at $t = 0$ to the value of the experimental condition and at $t = 20$ back to zero, in order to simulate receptor internalisation and to avoid oscillations. Both SQUAD and HillCube formalisms include Hill-coefficients which represent the cooperativity behaviour of the respective interaction. For the sake of parameter reduction, we included in both cases only one Hill-coefficient into parameter estimation, which is valid for all reactions and can be interpreted as the average cooperativity of

the whole system. More information about the mathematical formalisms and the applied parameters can be found in the methods section.

Fig. 2 shows the measured data together with the respective trajectories of all three models.

A comprehensive time-resolved detection of aggregation by light scattering after stimulation with different concentrations of ADP was applied to capture the aggregation dynamics (Fig. 2A–C). The analysis reveals a clear threshold behaviour dependent on the concentration of ADP. At low concentrations the system exhibits a transient activation and quickly regresses to the ground state. High concentrations of ADP lead to threshold transgression and a sustained aggregation. At medium concentrations the measurements show an initial reversibility. Here, the on/off decision is dependent on the complementary effect of autocrine thromboxan signaling, which acts as a delayed positive feedback loop. Model 1 (Fig. 2A) describes the whole dataset in an adequate manner.
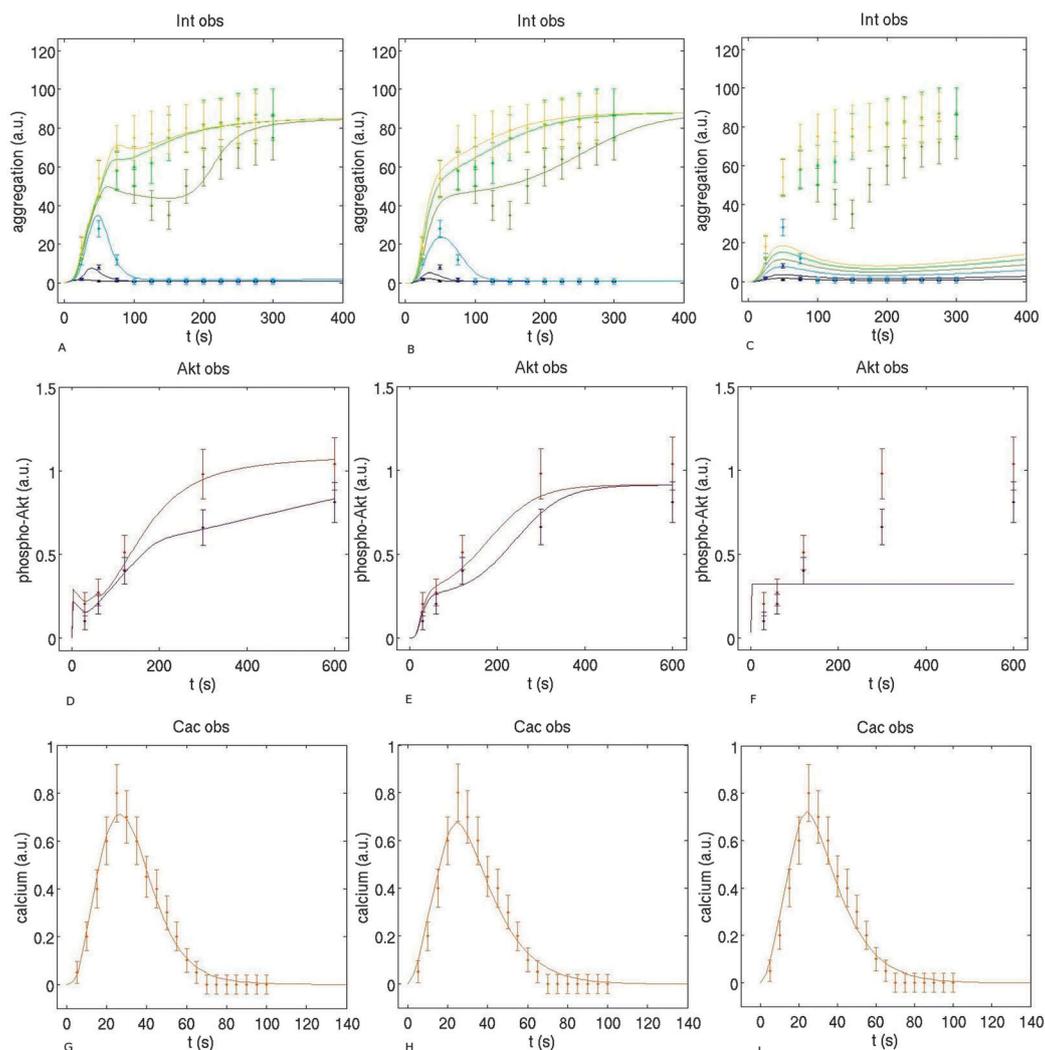
Fig. 2 Experimental data and model trajectories. All three models are compared (SQUAD model: three left panels) using the same set of experimental data. (A–C) LASCA-based aggregation measurement after ADP stimulation (A: SQUAD, B: HillCube, C: mass-action, yellow: 5 μM, light green: 1 μM, green: 0.8 μM, light blue: 0.6 μM, blue: 0.4 μM, black: 0.2 μM) (D and F) Akt measurement after ADP stimulation (red) and ADP stimulation in the presence of 10 nM ARC (purple) (D: SQUAD, E: HillCube, F: mass-action) (G—I): calcium measurement after ADP stimulation (G: SQUAD, H: HillCube, I: mass-action).

Model 2 (Fig. 2B) is able to reproduce the threshold behaviour, but performs worse in the medium and low concentration range compared to the SQUAD approach. Model 3 (Fig. 2C) fails to fit the data.

Fig. 2D–F shows a western-blot detection of phosphorylated Akt kinase (blot scanned and quantified) after ADP stimulation either in the presence or absence of 10 μM ARC.

In both logic ODE models the trajectory of Akt kinase shows a strong followed by a weaker increase. In the SQUAD model, this transition is interrupted by a slight drop which is not resolved by the experimental data. This behaviour results from a decreasing PI3 kinase activity as ADP-bound P2Y12 becomes internalised. The second increase is due to the activation of Src kinase and the bistability switch, which takes integrin outside-in signaling as input and is well visible in the experimental data. The observed dynamics in the presence of the P2Y12 antagonist ARC are comparable to those without ARC, but on a lower scale. Model 1 (Fig. 2D) displays a clear separation of the two trajectories, whereas in model 2 (Fig. 2E) both conditions end up in the same steady state after 8 minutes, which is not consistent with the data. Also in this case the mass action model fails to deliver an appropriate description of the data.

The Fig. 2G–I show a measurement of cytosolic calcium that displays a transient rise with a peak at the 8-fold basal concentration. All three models are able to fit this data.

Table 1 assigns the three models to their corresponding χ^2-values. Parameter estimation was conducted with respect to all experimental conditions simultaneously. We found that model 1 displays the smallest model-to-data distance ($\chi^2/N = 0.82$), followed by model 2 ($\chi^2/N = 1.74$) and model 3 ($\chi^2/N = 11.63$), after 1000 fits with $N = 106$ in all three cases. This result becomes even more convincing when the number of fitted parameters is taken into account, which is 35 for the SQUAD model, 41 for the HillCube model and 52 for the mass-action model. In the latter case we experimented with the model structure and the number of fitted parameters, but came to the conclusion, that even in an overparameterized shape, a mass-action formalism does not seem to capture the measured dynamics in an appropriate manner. The result suggests logic ODEs, in particular the standardized qualitative dynamical systems approach, in combination with parameter estimation to be a better choice to model platelet bistability than mass action approaches. One explanation could be, that both SQUAD and HillCube approaches descent from Boolean modeling, which is based on discrete alternations between the values 0 and 1. Thus, bistability holds for each individual node. In our platelet model, the overall system-state is dependent on the activation of either Src or PTP, that means a local bistability is

directly transferred to a global one. This may represent a convenient scenario for a Boolean-derived approach. Another explanation may result from the generalized form of the differential equations. The exact kinetics, by which a group of Src kinases interacts with a group of tyrosine phosphatases are unkown and may be too complex to be described by a simple mass action or Michaelis–Menten mechanism. Regarding the better performance of the SQUAD model then the HillCube approach we directly observe that the interpolation function works better in the example studied. e-functions are quite generic and deliver a good fit under many tasks including this one. However, this of course also depends on the specific problem modelled. Thus, the inherent threshold behaviour was analyzed using the SQUAD-based ODE-modeling approach. Profile likelihood analysis revealed all parameters of this model to be identifiable using point-wise confidence intervals. However, in its generality the question for the best modeling approach can not be answered as it is always dependent on the precise problem structure. Thus, several approaches should be compared in order to describe the respective system with least model-to-data distance.

Dynamical properties of the Src-PTP bistability switch

The interplay between Src-kinase and its deactivating tyrosine phosphatases represents the key element of platelet bistability.

In order to switch from reversible to irreversible aggregation, a substantial amount of Src molecules in the platelet cytoplasm needs to be phosphorylated to outcompete the inhibitory effect of the phosphatases. This is achieved by prolonged outside-in signaling from the activated integrin and subsequent auto-phosphorylation of tyr-416. Activated Src in turn phosphorylates the phosphatases in an inhibitory manner. The kinetic rates of this phosphorylation–dephosphorylation cycles were determined by parameter estimation and subjected to identifiability analysis. Table 2 shows the fitted parameters of model 1 along with their point-wise confidence intervals. All parameters can be interpreted as biochemical turn-over numbers and thus have the dimension s^{-1}. It shows that the self-activation rate of Src (Src_Src) is with its value of 3.51 significantly higher than that of PTP (PTP_PTP), which is 0.002. On the other hand, Src deactivates PTP (PTP_Src) with a much lower strength, than *vice versa* (Src_PTP) (2.19 compared to 29 479). The model also includes a stability parameter for each node, which represents the quotient of degradation and synthesis. This parameter is for PTP by a factor of 17 higher

Table 1 Model-to-data distances of the three implementations with $N = 106$ data points

Model	Chi^2/N	Free parameters
1 (SQUAD)	0.82	35
2 (HillCube)	1.74	41
3 (Mass-action)	11.63	55

Table 2 Bistability parameters and their respective confidence intervals of model 1

Parameter	Value	Lower border	Upper border
Src_Src	3.51	2.11	4.87
Src_PTP	29 479	28 752	36 643
Src$_{stab}$	0.47	0.039	4.17
PTP_PTP	0.002	0.00016	0.0099
PTP_Src	2.19	1.02	8.56
PTP$_{stab}$	5.9	3.13	6.99
Src$_{eff}$	16.3	Not fitted	Not fitted
PTP$_{eff}$	9.99	Not fitted	Not fitted

than for Src. The factors Src$_{eff}$ and PTP$_{eff}$ stand for the overall effectiveness of Src and PTP and are calculated using the following formula:

$$k_{eff} = \frac{k_{aut} \cdot k_{inh}}{k_{sta}}$$

k_{aut} represents the self-activation rate, k_{inh} the strength of the inhibition effect on the other node and k_{sta} the stability parameter. The effectiveness merges the dynamical properties of Src and PTP and is for both nodes in the same order of magnitude (16.35 and 9.99), even though the individual parameters differ within a very broad range. However, Src displays a slightly higher effectiveness than PTP, indicating the system's architecture to guarantee a fast and reliable response in the presence of a sufficiently high stimulus.

Validation

We validated our model by two additional datasets that had not been used in any of the steps before. The first dataset comprises a western-blot measurement of activated Rap1 after stimulation with ADP. Rap1 represents a downstream effector of calcium signaling and directly transmits the signal to integrin α2bβ3.

The dynamics of Rap1 activation were measured by GTP-pulldown assay combined with western-blotting. They display a fast increase followed by successive deactivation (Fig. 3A). The SQUAD and HillCube models accurately reproduce these data on Rap1 activation (red and black). However, there are differences in the predicted dynamics. In the HillCube model the trajectory of activated Rap1 displays a very fast increase followed by a short plateau where the activation level stays constant and a subsequent steep drop, leading to complete inactivation after 100 seconds. The SQUAD model on the other hand shows a less fast increase followed by a clear peak lying 0.2 arbitrary units higher than the HillCube plateau. Here, the deactivation progresses slower, a complete loss of Rap1 engagement can be observed after 250 seconds. Both trajectories fall within the predicted error bars, a final rating can not be made on the basis of the measured data. Though the mass action model shows comparable Rap1 dynamics, its trajectory displays both a weaker increase and decrease, and is thus not able to describe the data accurately.

The second dataset represents a time-resolved LASCA-based aggregation detection after ADP stimulation in the presence of MRS, which is a selective P2Y1 antagonist. In this scenario, the system becomes partially activated and assumes an in-between steady-state. This indicates, that for threshold formation a coordinated signaling through both ADP receptors is necessary (Fig. 3B). In this scenario, the SQUAD model predicts a slightly stronger increase compared to the data, followed by a decent drop, and thus does not reproduce the measurements perfectly. However, it accurately depicts the threshold disruption embodied by the in-between steady-state. Here, both HillCube and mass action models fail to fit the data. Another possibility for validation would have been to split the training dataset and use one steady-state for parameter estimation and the other for verification. Since the occurrence of bistability as a model property is not only dependent on the shape of the equations,
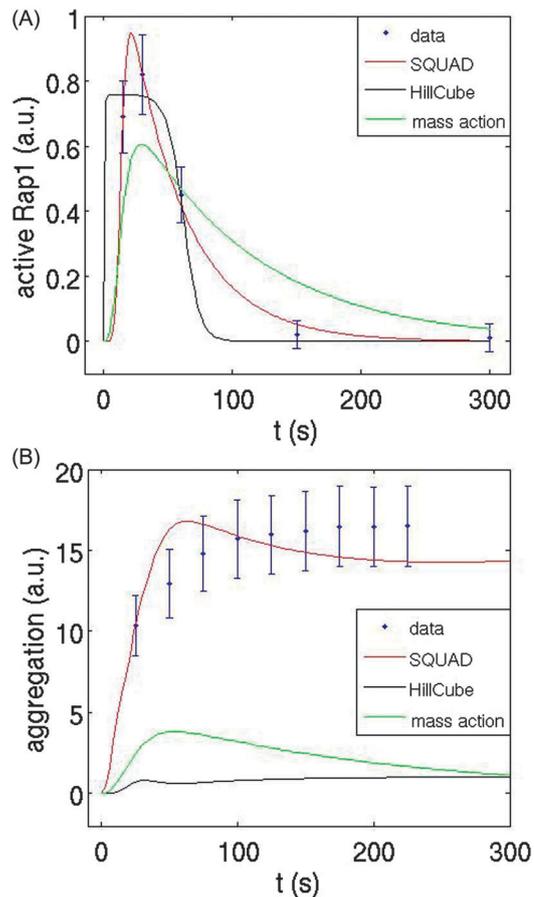

Fig. 3 Validation. (A) Rap1 measurement after ADP stimulation (0.6 μM). (B) LASCA-based aggregation measurement after ADP stimulation in the presence of MRS (50 μM). Colours distinguish model trajectories of different model approaches.

but also on the applied parameters, we needed data about both steady states in order to calibrate the model to a region of the parameter space that allows for bistability. Furthermore, using only one steady-state for optimization instead of two would have severely enlarged the parameters' confidence intervals. Thus, we decided to validate the model as shown in Fig. 3.

Model implications and applications

Existing models of platelet function comprise calcium and phosphoinositide dynamics,[13] PAR1 signaling,[8] prostaglandin signaling,[6] cAMP/cGMP turnover[9] and Boolean logic for subnetwork activation.[5] Regarding platelet aggregation, many studies appeared (reviewed in 1, 2). The system's inherent bistability, however, has never been elucidated by means of data-based modeling so far. Using our models, we provide a quantitative analysis of the threshold representing the transition from reversible to irreversible aggregation, assess the identifiability of the estimated parameters and validate our results with additional datasets. Though of course simplified, the model suggests also future targets for further antithrombotic research: Src kinase as pivotal engine in signal transmission is difficult to modify as kinase inhibitors (including Akt inhibition for instance)

are not so specific and side-effects in other cell types containing Src or Akt are high. However, we show that a set of protein tyrosine phosphatases (PTPs) is instrumental in platelets to regulate the response avalanche and here a pharmacological intervention should be considered and targeted in a platelet-specific way. Furthermore, our model helps to better understand dosage effects of platelet inhibitors already in use such as P2Y12 antagonists (such as Clopidogrel and Prasugrel) and this again alone or in combination with other platelet agonists and antagonists.

Conclusion

Ordinary differential equations model dynamical properties of biological systems, provided detailed information on underlying reaction kinetics is available. To model the complex bistability switch in platelets with a limited amount of experimental data we introduce here logic ODEs derived from Boolean expressions and exploit datasets on high sensitive LASCA measurements on aggregation. Logic ODEs abstain from including detailed reaction kinetics, but focus on the information given by the network topology. We show how corresponding equations can automatically be inferred by suitable scripts, this simplifies and shortens model-based hypothesis testing. Our Boolean ODE formalism on platelet activation shows how key platelet components combine to achieve a bistability switch, and points out involved pathways and potential targets for medical intervention. Obtained detailed kinetics of platelet aggregation allows to simulate modulation by clinical important aggregation antagonists such as Clopidogrel and Prasugrel. Future models will also include the inhibitory cAMP/PKA pathway to gain a more comprehensive view of the network dynamics.

Acknowledgements

Notes and references

1 Z. M. Ruggeri and G. L. Mendolicchio, *Circ. Res.*, 2007, **100**(12), 1673–1685.

2 T. A. Meadows and D. L. Bhatt, *Circ. Res.*, 2007, **100**(9), 1261–1275.

3 C. Gachet, *Thromb. Haemostasis*, 2008, **99**(3), 466–472, DOI: 10.1160/TH07-11-0673.

4 A. D. Michelson, *Arterioscler. Thromb. Vasc. Biol.*, 2008, **28**(3), s33–s38, DOI: 10.1161/ATVBAHA.107.160689, Epub 2008 Jan 3.

5 M. Mischnik, D. Boyanova, K. Hubertus, J. Geiger, N. Philippi, M. Dittrich, G. Wangorsch, J. Timmer and T. Dandekar, *Mol. BioSyst.*, 2013, **9**(6), 1326–1339, DOI: 10.1039/c3mb25597b, Epub 2013 Mar 6.

6 M. Mischnik, K. Hubertus, J. Geiger, T. Dandekar and J. Timmer, *Mol. BioSyst.*, 2013, **9**(10), 2520–2529, DOI: 10.1039/c3mb70142e.

7 J. E. Purvis, M. S. Chatterjee, l. F. Brass and S. L. Diamond, *Blood*, 2008, **112**(10), 4069–4079.

8 L. Lenoci, M. Duvernay, S. Satchell, E. DiBenedetto and H. E. Hamm, *Mol. BioSyst.*, 2011, **7**(4), 1129–1137, DOI: 10.1039/c0mb00250j, Epub 2011 Jan 12.

9 G. Wangorsch, E. Butt, R. Mark, K. Hubertus, J. Geiger, T. Dandekar and M. Dittrich, *BMC Syst. Biol.*, 2011, **5**, 178, DOI: 10.1186/1752-0509-5-178.

10 L. Mendoza and I. Xenarios, *Theor. Biol. Med. Model.*, 2006, **3**, 13.

11 D. M. Wittmann, J. Krumsiek, J. Saez-Rodriguez, D. A. Lauffenburger, S. Klamt and F. J. Theis, *BMC Syst. Biol.*, 2009, **3**, 98, DOI: 10.1186/1752-0509-3-98.

12 F. Thomas and L. Yuying, *SIAM J. Optim.*, 1996, **6**(2), 418–445.

13 A. Hindmarsh, P. Brown, K. Grant, S. Lee, R. Serban, D. Shumaker and C. Woodward, *ACM Transactions on Mathematical Software*, 2005, **31**(3), 363–396.

14 T. Maiwald and J. Timmer, *Bioinformatics*, 2008, **24**(18), 2037–2043, DOI: 10.1093/bioinformatics/btn350, Epub 2008 Jul 9.

15 A. Raue, C. Kreutz, T. Maiwald, J. Bachmann, M. Schilling, U. Klingmüller and J. Timmer, *Bioinformatics*, 2009, **25**(15), 1923–1929, DOI: 10.1093/bioinformatics/btp358, Epub 2009 Jun 8.

16 H. Subramanian, R. P. Zahedi, A. Sickmann, U. Walter and S. Gambaryan, *J. Thromb. Haemost.*, 2013, **11**(8), 1574–1582, DOI: 10.1111/jth.12271.

17 I. Mindukshev, S. Gambaryan, L. Kehrer, C. Schuetz, A. Kobsar, N. Rukoyatkina, V. O. Nikolaev, A. Krivchenko, S. P. Watson, U. Walter and J. Geiger, *Clin. Chem. Lab. Med.*, 2012, **50**(7), 1253–1262.